ACS OMEGA

http://pubs.acs.org/journal/acsodf

Article

Thermal Properties and Reliabilities of Lauric Acid-Based Binary Eutectic Fatty Acid as a Phase Change Material for Building Energy Conservation

Zhixuan Fan, Yunchao Zhao,* Xuying Liu, Yu Shi, and Dahua Jiang

Cite This: *ACS Omega* 2022, 7, 16097−16108

Read Online

ACCESS | Metrics & More | Article Recommendations

ABSTRACT: Thermal properties, stability, and reliability of lauric acid-based binary eutectic mixtures for building energy efficiency were studied. The eutectic points and phase change performance of these binary PCMs were obtained as follows: (1) For lauric acid−myristic acid, the mass eutectic point is 70 wt % LA/30 wt % MA. (2) For lauric acid−palmitic acid, the eutectic point is 79 wt % LA/21 wt % PA. (3) For lauric acid−stearic acid, the eutectic point is 82 wt % LA/18 wt % SA. The eutectic PCMs have a melting enthalpy of 166.18, 183.07, and 189.50 J·g^{-1} and a melting temperature of 35.10, 37.15, and 39.29 °C for lauric−myristic acid, lauric−palmitic acid, and lauric−stearic acid binary eutectic PCMs, respectively. The experimental results are very close to the theoretical results. Moreover, from FT-IR and XRD investigations, we realized that during the preparation of the lauric acid-based binary eutectic fatty acids, no new functional groups were produced. Besides, the TG illustrated that the LA−MA eutectic PCMs, LA−PA eutectic PCMs, and LA−SA eutectic PCMs exhibit excellent thermal stability below 126.51, 135.7, and 110.08 °C, respectively. Finally, lauric acid-based binary eutectic PCMs still show excellent thermal properties and chemical structure after 500 hot and cold cycles. All in all, as a novel material for building energy conservation, lauric acid-based binary eutectic PCMs have broad prospects and good practicability.

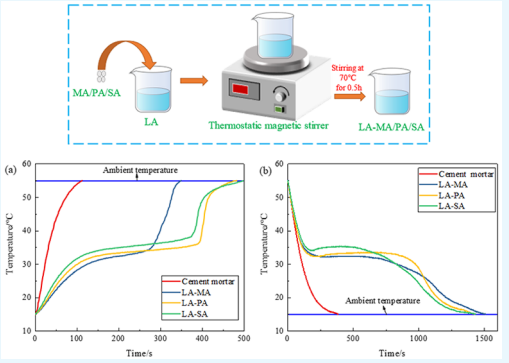

1. INTRODUCTION

With the prosperity of the global economy and industry, solving the problems of carbon emissions and the lack of fossil fuel is of great significance to society.[1] These problems are related to the increasing global energy consumption. Buildings consume about one-third of global energy consumption.[2] Thus, building energy conservation is one of the effective measures to solve carbon emissions and the lack of fossil fuel. Phase change materials (PCMs) can store or liberate massive enthalpy during the melting or solidification process while keeping its own temperature constant, which have been extensively used in building walls, roofs, floors, solar energy collection, and so on.[3−8] PCMs include organic, inorganic, and mixed PCMs. Furthermore, organic PCMs have been classified into the following: paraffin, fatty acids, alcohols, and lipids. In organic PCMs that have been studied, fatty acids are biological compounds extracted from food and oils under certain conditions and can be continuously supplied in the absence of fossil fuel sources.[9,10] They have good development prospects on account of the following advantages: high heat capacity, very slight or no supercoiling, nontoxic, noncorrosive, excellent thermal and chemical stability, small volume change during phase transformation, appropriate melting temperature range for building energy conservation, and so on.[11−16] Nevertheless, the melting temperature of pure fatty acids is too simple to be suitable for building energy conservation; the initial melting temperature of capric acid (CA), lauric acid (LA), myristic acid (MA), palmitic acid (PA), and stearic acid (SA) are about 31, 43, 54, 62, and 69 °C,[17] but heaven always leaves one way out. In previous studies, it was found that eutectic PCMs with a lower phase transition temperature can be prepared by mixing two or more PCMs. Many researchers believe that the fatty acid eutectic mixtures have ideal characteristics for building energy conservation. For example, Saeed[18] had prepared and investigated binary eutectic PCMs, which are composed of methyl palmitate (MP) and LA. It was found that the phase change temperature, subcooling, and enthalpy of MP-LA are 25.6 °C, 0.7 °C, and 205.4 J·g^{-1}, respectively. Wen et al.[19] mixed CA and LA to form CA−LA and found its melting temperature and enthalpy are 19.1 °C and 141.5 J·g^{-1}. Khawaji et al.[20] studied a eutectic mixture of CA and MA, of which the phase transition

Received: March 9, 2022
Accepted: April 15, 2022
Published: April 27, 2022

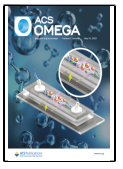

https://doi.org/10.1021/acsomega.2c01420
ACS Omega 2022, 7, 16097−16108

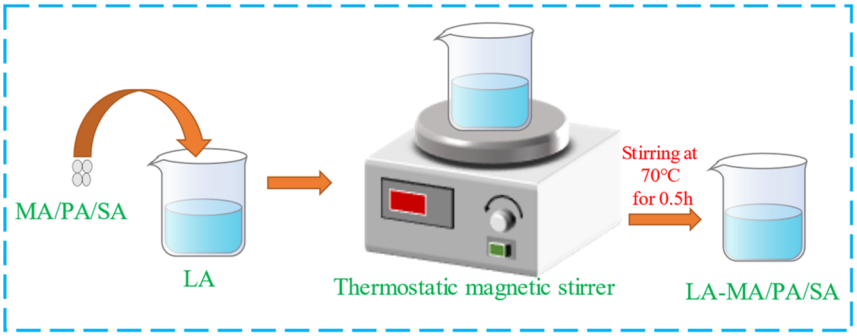

Figure 1. Schematic diagram of the preparation process.

temperature is 25.6 °C and the enthalpy is 205.4 $J \cdot g^{-1}$. Moreover, they concluded that this material is of critical significance for temperature control in buildings. Based on DSC results, Han[21] found that a eutectic mixture of LA and 1,6-hexanediol (HE), when the mass percentage of LA is 70%, displays a lower phase transition temperature and good stability after 1000 cycles. Recently, some scholars have studied eutectic PCMs with a phase transition temperature range from 19 to 27 °C.[22] However, according to refs 23−25, the optimum phase transition temperature is different in different climatic regions. A higher phase transition temperature range can significantly reduce energy consumption in the summer for areas with high average temperatures. But the eutectic PCMs with the phase transition temperature range of 35−40 °C have received less attention than the temperature of 18−30 °C. Lauric acid, a fatty acid PCM, has the advantages that all these fatty acids have. In addition, with its unique phase change temperature of approximately 43 °C, it can be combined with many organic materials to obtain a phase change temperature and high latent heat suitable for the construction sector. Many scholars combined some lauric acid-based phase change materials with building materials by technical means to study the energy-saving effect of composite materials. For example, Hekimoğlu[26] added lauric acid−myristic acid fly ash/composite to standard cement mortar to prepare phase change cement and compared the thermal performance test with standard cement. The results show that the temperature of the phase change mortar is lower than that of the standard mortar during the heating process, and the prepared phase change mortar has a good energy-saving effect. There are also studies on LA-based binary eutectic PCMs, for instance, Sarı[27] experimentally determined the eutectic point of LA−MA and LA−PA and reported their thermal properties and thermal reliability. It was concluded that LA−MA and LA−PA have excellent thermal properties and thermal reliability. Ke[28] obtained the eutectic ratios of almost all eutectic fatty acids by theoretical calculations and reported their thermal properties and chemical structures. However, they used only one of theory or experiment to determine the eutectic point, and they neglected the comparative analysis of the theoretical and experimental eutectic points. Moreover, they did not focus on the crystal structure, thermal stability, and comparative analysis of the heat resistance of LA-based binary eutectic PCMs.

Therefore, in this paper, LA whose phase transition temperature is slightly higher than this temperature range of 35−40 °C was selected as the main component. MA, PA, and SA, with higher enthalpy, are respectively selected as the second component. The lauric acid-based PCMs are prepared by mixing the main component and the second component. The thermophysical properties of LA, MA, PA, SA, and their mixtures were examined by differential scanning calorimetry (DSC), the step cold test, heat resistance test, and thermogravimetry (TG) analysis. The chemical and crystal structure of LA, MA, PA, SA, and their eutectic mixtures were evaluated by X-ray diffraction (XRD) and Fourier transform infrared spectroscopy (FT-IR). Thermal resistance analyses of LA-MA, LA-PA and LA-SA were performed. Furthermore, after an accelerated thermal cycling test of these binary eutectic PCMs, their thermal and chemical reliabilities were investigated by using DSC and FT-IR.

2. MATERIALS AND METHODS

2.1. Materials. Lauric acid (LA, $C_{12}H_{24}O_2$, 172.2, AR) was purchased from Shandong Yousuo Compound Engineering Co., Ltd. (Shandong, China). Myristic acid (MA, $C_{14}H_{28}O_2$, 228.37, AR), palmitic acid (PA, $C_{16}H_{32}O_2$, 256.42, AR), and stearic acid (SA, $C_{18}H_{36}O_2$, 284.48, AR) were bought starting with Sinopharm Concoction Reagent Co., Ltd. (Shanghai, China). These chemicals were utilized without further depuration.

2.2. Preparation of LA-Based Binary Mixtures. LA−MA binary mixtures were prepared as follows. In the first instance, LA and MA with a certain mass ratio were weighed in a beaker, sealing them with a film. Second, the beaker was put into a water bath magnetic stirrer with a temperature of 70 °C. In the end, the mixture was stirred for 0.5 h after it was melted to ensure uniform mixing. LA−MA binary eutectic mixtures with different LA mass percentages were prepared. The preparation process of the binary eutectic mixtures LA−PA and LA−-SA was similar to the above steps, and the schematic diagram of the preparation process is shown in Figure 1.

2.3. Characterization. The temperature−time curve of the samples drops from 80 to 10 °C was recorded using a temperature detector (Agilent 34972A, accuracy is ±0.5 °C) with a time step of 60 s. The phase transition temperature and phase transition enthalpy of the samples were determined using a differential scanning calorimeter (DSC, Mettler DSC1) at a flow rate of nitrogen of 50 mL/min, with a ramp-up and ramp-down rate of 5 °C/min. The chemical structure of the samples was characterized by Fourier transmission and infrared spectroscopy (FT-IR, PerkinElmer Frontier Model, U.S.A.) using KBr pellets. The scanning range was 600−4000 cm^{-1}. The crystal structure of the samples before and after mixing was characterized by X-ray diffraction (XRD, PANalytical B.V., Netherlands), the scan range of this analysis was 10−80°, and the scan rate was 3°/min. The thermal stability of the samples was investigated by thermal gravimetric analysis (TGA, Q500, TA Company, U.S.A.) in a nitrogen atmosphere that was heated from 30 to 400 °C at a temperature increase rate of 10 K/min. The thermal cycling experiment was performed by heating the

https://doi.org/10.1021/acsomega.2c01420
ACS Omega 2022, 7, 16097−16108

PCMs to 60 °C and then cooling them to 10 °C, with the PCMs passing through 500 cycles of accelerated heating and cooling, and the thermal properties of the samples after 100, 200, 300, and 500 cycles were compared with those before the cycle. FTIR analysis was performed to compare the chemical structure of the samples after 500 cycles with that of samples after 1 cycle.

2.4. Model and Correlation. The Schroder's equations,[29] shown in eq 1, were used to calculate the eutectic point and the phase transition temperature of the binary mixtures. For organic PCMs with a larger molecular weight, eq 2[30] can be used to calculate the phase transition enthalpy of the binary mixtures.

$$T_m = \frac{T_i \Delta H_i}{\Delta H_i - R T_i \ln X_i} \quad (1)$$

$$\Delta H_m = T_m \sum_{i=1}^{n} \frac{X_i \Delta H_i}{T_i} \quad (2)$$

where T_m is the melting temperature of the binary mixture, K; T_i is the melting temperature of the pure material i; ΔH_m is the melting enthalpy of the mixture, J/mol; ΔH_i is the melting enthalpy of the pure material i, J/mol; X_i is the mole percentage of the pure material i; R = 8.315 J/(mol·K).

3. RESULTS AND DISCUSSION

3.1. Thermal Properties of the Pure Fatty Acids. The step cooling and DSC curve of the pure fatty acids were presented in Figures 2 and 3, respectively. First, it can be seen

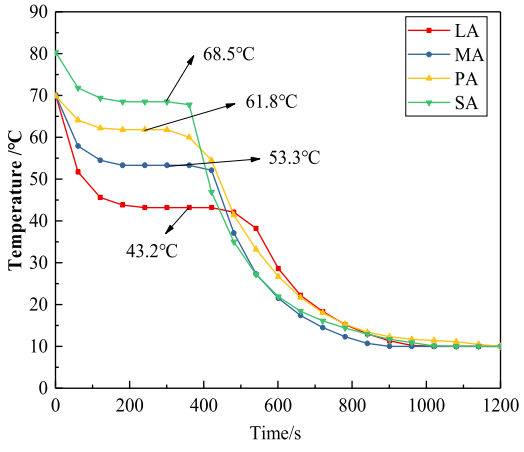

Figure 2. Step cooling curves of pure fatty acids.

from Figure 2, the freezing temperature of LA, MA, PA, and SA is 43.2, 53.3, 61.8, and 68.5 °C, respectively. Moreover, similar results were verified in the DSC curve shown in Figure 3, with the corresponding data of the melting temperature (T_m), the freezing temperature (T_f), the melting enthalpy (ΔH_m), and the freezing enthalpy (ΔH_f) presented in Table 1. It is found that the phase transition temperature and enthalpy of the pure fatty acids increase with the number of carbon atoms. The explanation of the phenomenon is as follows: as a molecular crystal, the intermolecular forces (mainly van der Waals forces in molecular crystals) significantly affect the phase change properties of the saturated fatty acids. The stronger the intermolecular forces, the higher the melting temperature required and the more thermal energy required for the melting process. Obviously, the increase in the number of carbon atoms leads to an increase in the number of electrons in the molecule, enhancing the van der

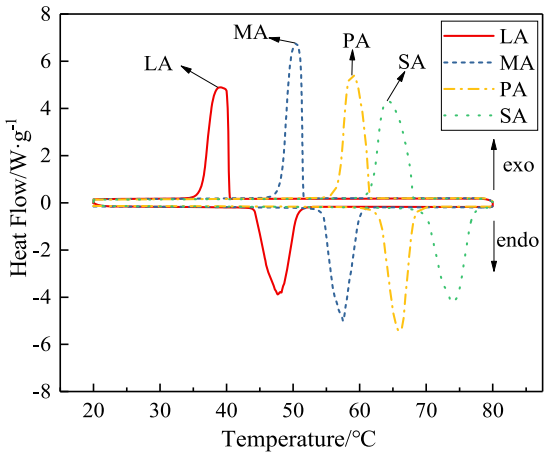

Figure 3. DSC curves of pure fatty acids.

Table 1. Thermal Phase Change Properties of Pure Fatty Acids

material	T_m (°C)	ΔH_m (J·g^{-1})	T_f (°C)	ΔH_f (J·g^{-1})
LA	43.93	178.11	40.63	178.98
MA	54.28	191.27	51.69	194.36
PA	62.73	206.16	61.64	204.56
SA	69.62	217.62	68.24	215.07

Waals force generated by electrostatic attraction. Therefore, the phase transition temperature and enthalpy of the pure fatty acids increase with the number of carbon atoms. The same pattern can be found in *n*-alkanes,[31] and many reported literature[17,28,32] also confirmed this law.

3.2. Determination of Eutectic Point of LA-Based Binary Phase Change Material. *3.2.1. Theoretical Prediction of Eutectic Point.* The solid−liquid phase diagram and melting enthalpy of the mixtures were calculated by eqs 1 and 2, as shown in Figure 4, and the calculation related data can be found in Table 1. As shown in Figure 4, first, the theoretical molar ratios of the LA−MA, LA−PA, and LA−SA binary eutectic mixtures were calculated at 65:35, 78:22, and 87:13, and the corresponding mass ratios were 62:11, 74:26, and 82:18. In addition, the theoretical melting temperatures of the LA−MA, LA−PA, and LA−SA binary eutectic mixtures were calculated as 34.16, 38.10, and 40.59 °C. Finally, the theoretical melting enthalpies of the LA−MA, LA−PA, and LA−SA binary eutectic mixtures are calculated as 175.25, 179.12, and 180.25 J·g^{-1}, respectively.

3.2.2. Experimental Eutectic Point. A series of mixtures near the theoretical ratio were prepared and measured. The mass ratio of the lowest freezing temperature is considered as the eutectic point; in addition, the plateau temperature in the cooling curve of the eutectic mixture is considered as its freezing temperature.

3.2.2.1. Eutectic Point of the LA−MA Mixture. The step cooling curves of LA−MA mixtures with different $\mathcal{M}_{LA}$ are indicated in Figure 5, where $\mathcal{M}_{LA}$ is the mass percentage of LA. As can be observed in Figure 5, when the mass percentage of LA is 66%, 68%, 69%, 70%, 71%, and 72%, the corresponding freezing temperature of the LA−MA mixture is 33.3, 33.1, 32.8, 32.6, 32.8, and 32.9 °C, respectively. The partial phase diagram of LA−MA was plotted in accordance with the data indicated in Figure 6. As indicated in Figure 6, the freezing temperature of the LA−MA binary mixture decreases with the increase of $\mathcal{M}_{LA}$

https://doi.org/10.1021/acsomega.2c01420
ACS Omega 2022, 7, 16097−16108

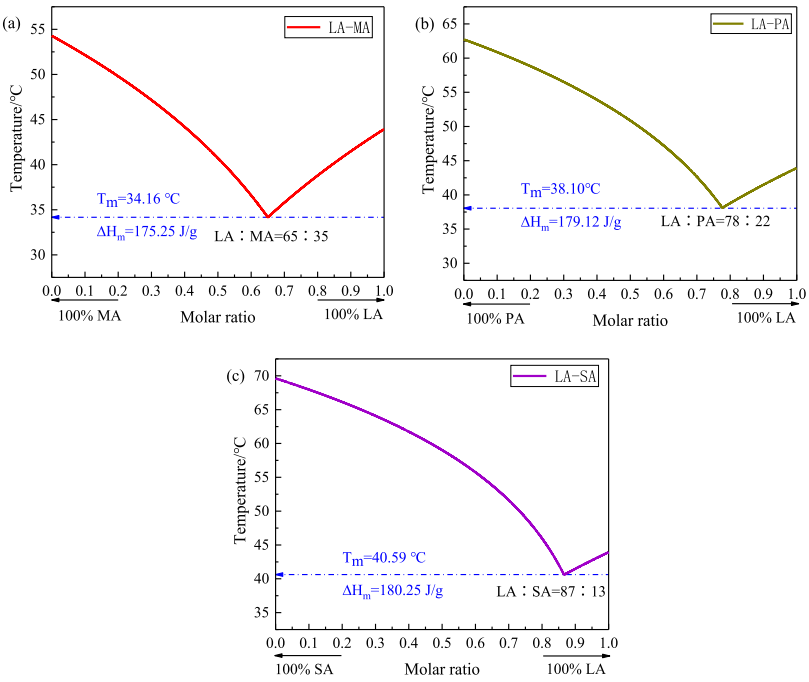

Figure 4. Phase diagrams of (a) LA−MA, (b) LA−PA, and (c) LA−SA binary mixtures.

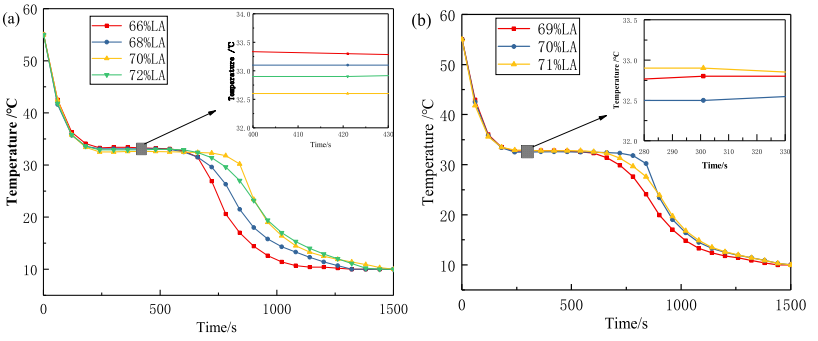

Figure 5. Step cooling curves of LA−MA with different $\mathcal{M}_{LA}$ values: (a) 66, 68, 70, and 72 wt % of LA and (b) 69, 70, and 71 wt % of LA.

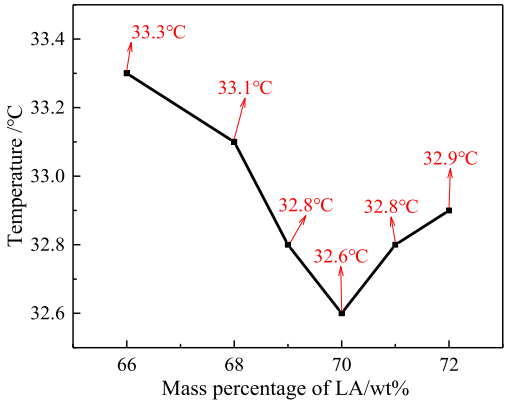

Figure 6. Partial phase diagram of the LA−MA.

at first and increases with the increase of $\mathcal{M}_{LA}$ after reaching the minimum value, which shows the same trend as the theoretical phase diagram. $\mathcal{M}_{LA}$ = 70% obviously corresponds to the lowest freezing temperature in the LA−MA mixtures. Therefore, we believe that $\mathcal{M}_{LA}$ = 70% is the eutectic point of the LA−MA mixture, and its freezing temperature is 32.6 °C.

3.2.2.2. Eutectic Point of the LA−PA Mixture. The step cooling curves of LA−PA binary mixtures with different $\mathcal{M}_{LA}$, as shown in Figure 7.

As shown in Figure 7, when $\mathcal{M}_{LA}$ is 72%, 74%, 76%, 78%, 79%, and 80%, the corresponding freezing temperature of the LA−PA

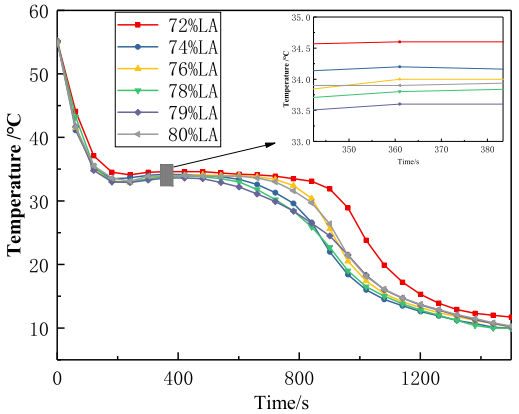

Figure 7. Step cooling curves of LA−PA with different $\mathcal{M}_{LA}$: 72, 74, 76, 78, 79, and 80 wt % of LA.

https://doi.org/10.1021/acsomega.2c01420
ACS Omega 2022, 7, 16097−16108

binary mixture is 34.6, 34.1, 34.0, 33.8, 33.6, and 33.9 °C, respectively. According to the above information indicated in Figure 7, the partial phase diagram of LA−PA is drawn in Figure 8. As shown in Figure 8, $\mathcal{M}_{LA}$ = 79% obviously corresponds to

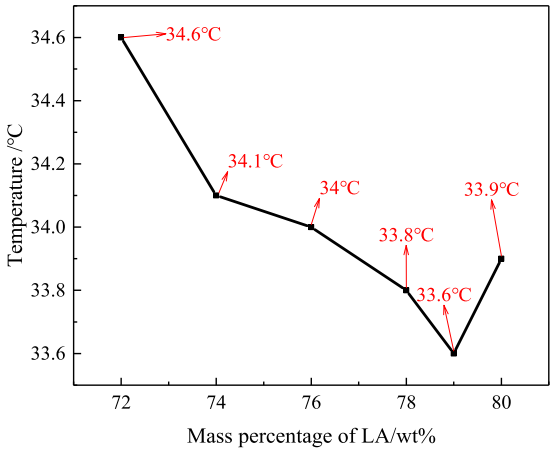

Figure 8. Partial phase diagram of the LA−PA.

the lowest freezing temperature in the LA−PA mixtures. Therefore, it is concluded that $\mathcal{M}_{LA}$ = 79% is the eutectic point of the LA−PA mixture, and its freezing temperature is 33.6 °C.

3.2.2.3. Eutectic Point of the LA−SA Mixture. The step cooling curves of the LA−SA mixture with different $\mathcal{M}_{LA}$ are indicated in Figure 9. Based on the information in Figure 9, when the mass percentage of LA is 76%, 80%, 81%, 82%, 83%, 84%, 88%, and 92%, the corresponding freezing temperature of the LA−PA binary mixture is 36.6, 35.6, 36.0, 34.7, 35.3, 35.6, 35.9, and 37.9 °C, respectively. According to the data indicated in Figure 9, the partial phase diagram of LA−PA is drawn in Figure 10. The freezing temperature of the LA−SA binary mixture with $\mathcal{M}_{LA}$ = 82% is the lowest, as shown in Figure 10. Therefore, it is concluded that $\mathcal{M}_{LA}$ = 82% is the eutectic point of the LA−SA mixture, and its freezing temperature is 34.7 °C.

3.3. Thermal Properties of Lauric Acid-Based Binary Eutectic PCMs. The thermal properties of LA−MA, LA−PA, and LA−SA eutectic PCMs were analyzed by DSC; their DSC curves are shown in Figure 11. From Figure 11 we can find that their DSC curves have only a single melting peak and a solidification peak. First of all, for LA−MA, as seen in Figure 11a, its melting temperature and enthalpy are 35.1 °C and 166.18 J·g^{-1}, respectively. The freezing temperature and enthalpy are 32.15 °C and 158.42 J·g^{-1}, respectively. Next, as shown in Figure

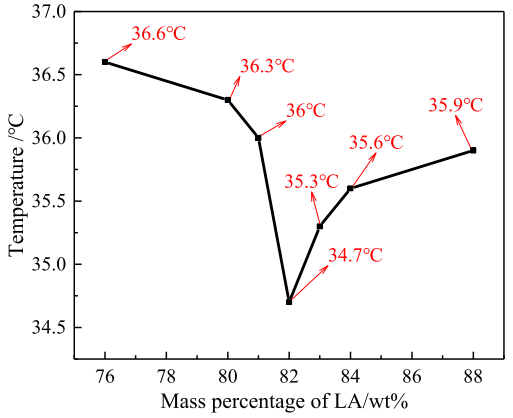

Figure 10. Partial phase diagram of LA−SA

11b, for LA−PA, the melting temperature and enthalpy are 37.15 °C and 183.07 J·g^{-1}, respectively, and the freezing temperature and enthalpy is 31.34 °C and 166.81 J·g^{-1}, respectively. In the end, as demonstrated in Figure 11c, the melting and freezing temperatures of the LA−SA eutectic PCMs are 39.29 and 32.44 °C, and the melting and freezing enthalpies are 189.5 and 176.15 J·g^{-1}. As stated by those eutectic theories, the phase transition characteristics of the eutectic binary mixture are fundamentally the same on single fatty acids, such as, it also has a single endothermic and exothermic peak. Hence, it is further verified that the LA−MA binary mixture with 70% LA mass percentage, the LA−PA binary mixture with 79% LA mass percentage, and the LA−SA binary mixture with 82% LA mass percentage are binary systems.

3.4. Correlation between Computational and Experimental Results. The computational and experimental values of each binary system are listed in Table 2. As shown in Table 2, the deviation between the computational and experimental eutectic points for LA−MA, LA−PA, and LA−SA mixtures was 0.08, 0.05, and 0, respectively. Likewise, the absolute deviation between the computational and experimental eutectic melting temperatures of LA−MA, LA−PA, and LA−SA binary mixturse was 0.94, 0.95, and 1.3 °C, respectively, and their relative deviations were 2.68%, 2.56% and 3.20%, respectively. Finally, the computational melting enthalpy was very close to the experimental, with absolute gap values of 9.07, 3.95, and 9.25 J·g^{-1} being noticed on the LA−MA, LA−PA, and LA−SA binary systems and their relative deviations being 5.46%, 2.16%, and 4.88%. In a word, the relative deviations of their various parameters are less than 10%. It is implied that eqs 1 and 2 have a

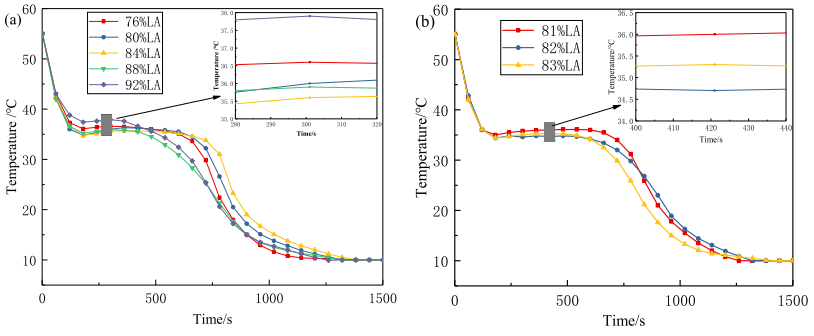

Figure 9. Step cooling curves of LA−SA with different $\mathcal{M}_{LA}$: (a) 76, 80, 84, 88, and 92 wt % of LA and (b) 81, 82, and 83 wt % of LA.

https://doi.org/10.1021/acsomega.2c01420
ACS Omega 2022, 7, 16097−16108

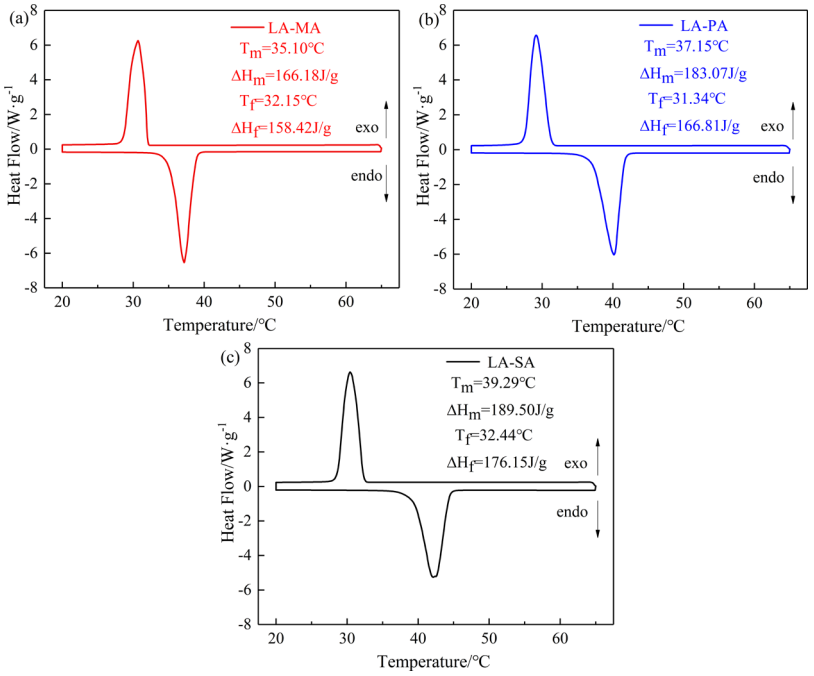

Figure 11. DSC curves of (a) LA−MA, (b) LA−PA, and (c) LA−SA binary eutectic PCMs.

Table 2. Computational and Experimental Values of the Thermal Properties for Each Binary Mixture

	computational values			experimental values		
eutectic PCMs	mass eutectic point	eutectic temp (°C)	melting enthalpy (J·g^{-1})	mass eutectic point	eutectic temp (°C)	melting enthalpy (J·g^{-1})
LA−MA	$\mathcal{M}_{LA}$ = 62%	34.16	175.25	$\mathcal{M}_{LA}$ = 70%	35.10	166.18
LA−PA	$\mathcal{M}_{LA}$ = 74%	38.10	179.12	$\mathcal{M}_{LA}$ = 79%	37.15	183.07
LA−SA	$\mathcal{M}_{LA}$ = 82%	40.59	180.25	$\mathcal{M}_{LA}$ = 82%	39.29	189.50

good predictive effect on the thermophysical parameters of the three eutectic systems.

3.5. Chemical Structures of LA-Based Binary Eutectic PCMs. The chemical changes of the eutectic mixtures after mixing were examined by FT-IR. The FT-IR spectra of the binary eutectic systems of LA−MA, LA−PA, and LA−SA are shown in Figure 12a−c, respectively.

The FTIR spectra of LA, MA, and LA−MA are given in Figure 12a. In the LA spectrum, the broad absorption band at 3300−2750 cm^{-1} of LA is the stretching vibration peak of −OH. The bands at 2920 and 2854 cm^{-1} are caused by the symmetric and asymmetric stretching vibration of $-CH_2$, respectively. The absorption peak caused by the stretching vibration of C═O appears at 1697 cm^{-1}, and the bending vibration of $-CH_2$ causes the absorption peak at 1464 cm^{-1}. The absorption peak at 1296 cm^{-1} is the in-plane bending vibration peak of −OH, the out-of-plane deformation vibration peak of −OH is at 939 cm^{-1}, and the absorption peak at 725 cm^{-1} represents the out-of-plane bending vibration of the C−H bond. In the FT-IR spectrum of MA, a pair of large peaks at 2918 and 2852 cm^{-1} are caused by the symmetric and asymmetric stretching vibrations of $-CH_2$, respectively. The characteristic absorption peak at 1699 cm^{-1} was caused by the stretching vibration of C═O, and the absorption peak at 1462 cm^{-1} was attributed to the asymmetric bending vibration of $-CH_2$. The absorption peak at 1297 cm^{-1} is the in-plane bending vibration peak of −OH, the out-of-plane deformation vibration peak of −OH is at 943 cm^{-1}, and the absorption peak at 723 cm^{-1} represents the out-of-plane bending vibration of the C−H bond. Similarly, in the FT-IR diagram of LA−MA, different characteristic absorption peaks appeared at 2921, 2852, 1699, 1464, 1296, 933, and 727 cm^{-1}. By observing the vertical line in the Figure 12a, we concluded that the main characteristic absorption peaks in the LA−MA spectrum could be found in the absorption peaks of LA or MA, with the deviation less than 6 cm^{-1}. In addition, no new characteristic peaks were found in the FT-IR spectra of LA−MA.

The FT-IR spectra of PA and LA−PA are shown in Figure 12b. As seen from the obtained spectrum of PA, the absorption peaks of PA are the same type as LA and MA, appearing at 2920, 2854, 1699, 1464, 1300, 941, and 725 cm^{-1}. In the same way, different absorption peaks appear at 2920, 2854, 1697, 1463, 1298, 937, and 724 cm^{-1} in the FT-IR spectrum of LA−PA. According to the FT-IR spectra of LA, PA, and LA−PA, it is found that the main absorption peaks of LA−PA can be found in the spectra of LA and PA, and the position deviation does not exceed 3 cm^{-1}. At the same time, there is no new characteristic peak in the spectrum of LA−PA eutectic system.

For the LA−SA eutectic system, the FT-IR spectra of SA and LA−SA are indicated in Figure 12c. The absorption peaks of SA are the same type as LA, MA, and PA, appearing at 2920, 2854, 1701, 1464, 1300, 945, and 725 cm^{-1} in the FT-IR spectrum of SA. Dependent upon the above information, it is concluded that the main absorption peaks of LA−SA can be found from the peaks of LA and SA, and the position deviation does not exceed 6 cm^{-1}. In addition, no new characteristic peaks appeared in the spectrum of LA−SA.

https://doi.org/10.1021/acsomega.2c01420
ACS Omega 2022, 7, 16097−16108

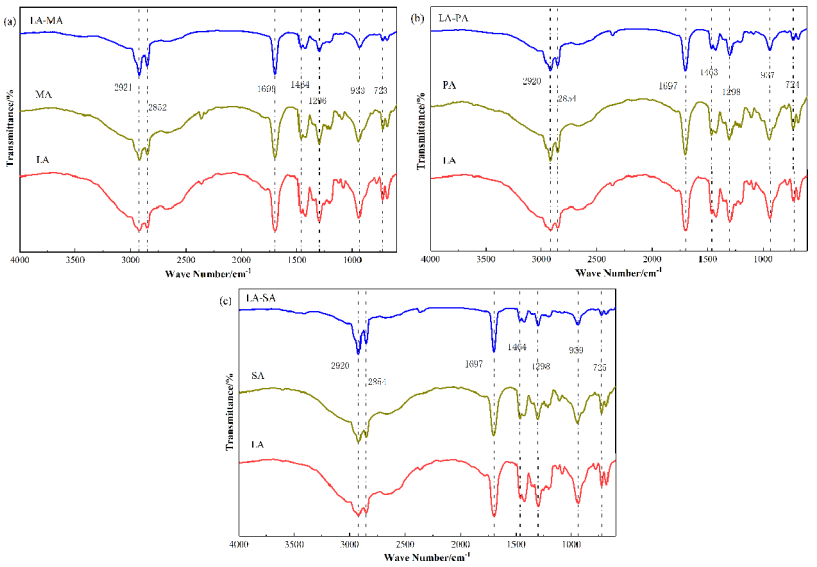

Figure 12. FT-IR spectra of (a) LA−MA, (b) LA−PA, and (c) LA−SA binary systems.

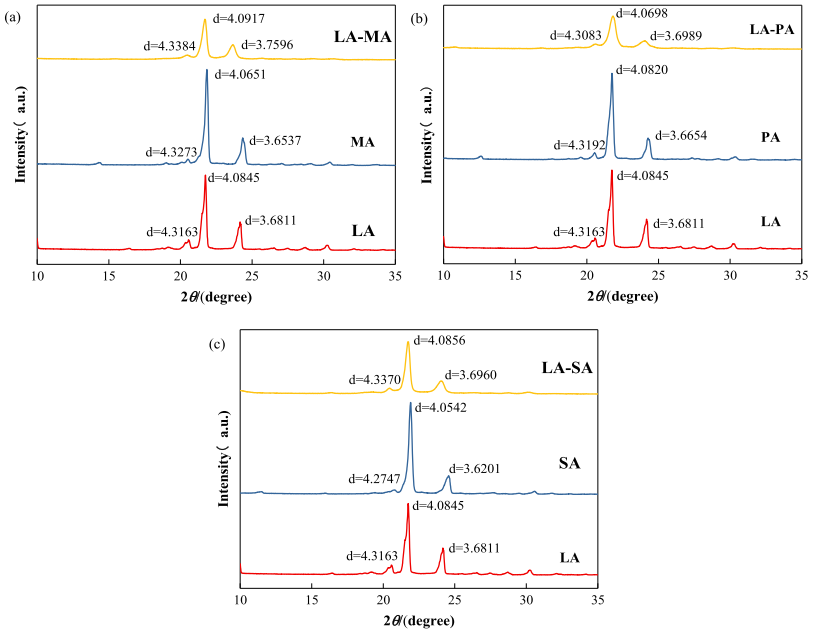

Figure 13. XRD curves of (a) LA−MA, (b) LA−PA, and (c) LA−SA binary systems.

The results show that LA−MA, LA−PA, and LA−SA are compounded by the physical interactions between LA and MA, PA, and SA, rather than chemical reactions.

3.6. Crystal Structure of LA-Based Binary Eutectic PCMs. XRD was used to evaluate the differences between the crystal structure of LA−MA, LA−PA, and LA−SA and the corresponding pure fatty acids. Their XRD patterns are shown in Figure 13.

As shown in Figure 13a, obviously, LA has three strong diffraction peaks at 2θ = 20.57°, 21.74°, and 24.16°, and the corresponding lattice distances are 4.3163, 4.0845, and 3.6811 Å, respectively. Furthermore, MA has three strong diffraction peaks at 2θ = 20.51°, 21.85°, and 24.34°, respectively, and the corresponding lattice distances are 4.3273, 4.0651, and 3.6537 Å. Moreover, LA−MA has diffraction peaks at 2θ = 20.45°, 21.70°, and 23.65°, and the corresponding lattice distances are 4.3384, 4.0917, and 3.7596 Å. By comparing the diffraction peak positions and lattice distances of LA, MA, and LA−MA, it is found that the diffraction peaks of LA and MA are very similar, and they exist in LA−MA. In addition, the diffraction peak angles changed from 20.57°, 21.74°, and 24.16° in LA to 20.51°, 21.85°, and 24.34° in MA to 20.45°, 21.70°, and 23.65° in LA−MA, and the maximum angular deviation does not exceed 0.7°. There are no new diffraction peaks in LA−MA. As shown in Figure 13b, the angles of these strong diffraction peaks of PA are respectively at 2θ = 20.55°, 21.74°, and 24.26°. Their corresponding lattice distances are 4.3192, 4.0820, and 3.6654 Å, respectively. Similarly, LA−PA has diffraction peaks at 2θ = 20.60°, 21.82°, and 24.04°, and the corresponding lattice distances are 4.3083, 4.0698, and 3.6989 Å. We found that LA and PA have similar diffraction peaks and both exist in LA−PA. The diffraction peak angles from 20.57°, 21.74°, and 24.16° in LA to 20.55°, 21.74° and 24.26° in PA to 20.60°, 21.82° and 24.04° in LA−PA, and the maximum angle gap does not exceed

https://doi.org/10.1021/acsomega.2c01420
ACS Omega 2022, 7, 16097−16108

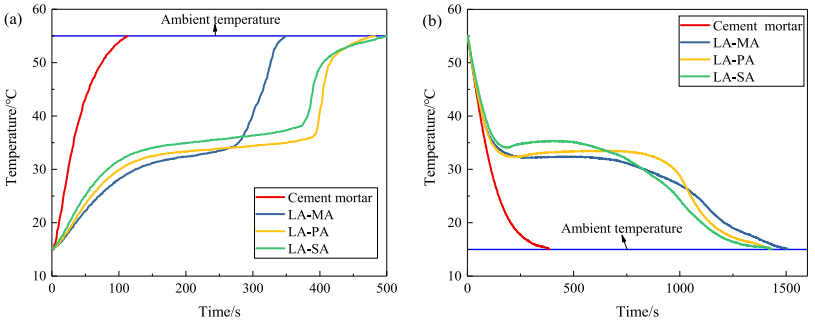

Figure 14. (a) Heating curves and (b) cooling curves of cement mortar, LA−MA, LA−PA, and LA−SA.

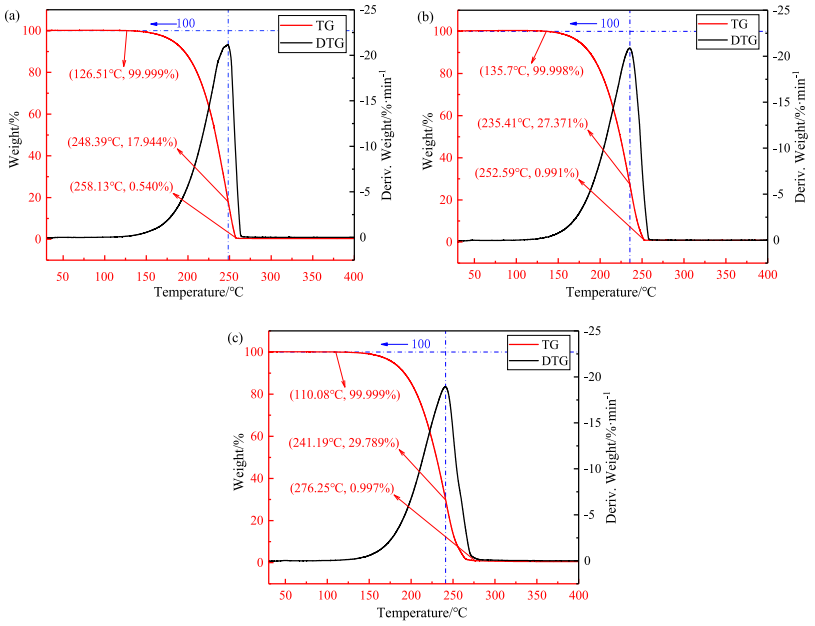

Figure 15. Thermogravimetric analysis curves of (a) LA−MA, (b) LA−PA, and (c) LA−SA binary eutectic PCMs.

0.3°. There are no new diffraction peaks in LA−PA. Observing Figure 13c, it is found that the three strong diffraction peak angles in SA are 2θ = 20.76°, 21.90°, and 24.56°, respectively. The corresponding lattice distances are 4.2747, 4.0542, and 3.6201 Å. Analogously, LA−SA has diffraction peaks at 2θ = 20.46°, 21.74°, and 24.06°, corresponding to the lattice distance of 4.3370, 4.0856, and 3.6960 Å. First of all, from the perspective of the peak shape, the diffraction peaks of LA and SA are very similar, and their diffraction peaks also exist in LA−SA. Second, the appearance angles of the peaks change from 20.57°, 21.74°, and 24.16° in LA to 20.76°, 21.90°, and 24.56° in SA to 20.46°, 21.74°, and 24.06° in LA−SA, respectively. Finally, there are no new diffraction peaks in LA−SA.

Therefore, the characteristic peaks in the XRD pattern of each binary eutectic PCM are derived from the pure fatty acids that make them up, which justified that LA and MA, LA and PA, and LA and SA are combined through physical molecular interactions rather than chemical reactions.

3.7. Comparative Analysis of Heat Resistance of Lauric Acid-Based Eutectic PCMs. We explored the feasibility of lauric acid-based binary eutectic PCMs as an energy-efficient building material by comparing the heating/cooling curves of lauric acid-based binary eutectic PCMs with conventional building materials (cement mortar). The experimental procedure is as follows, as well as the experimental results are shown in Figure 14. First, four test tubes containing 10 g of cement mortar, LA−MA, LA−PA, and LA−SA were placed in a constant temperature incubator at 15 °C. When the temperature of all the test tubes dropped to 15 °C, the test tubes were removed and placed in a constant temperature water tank at 55 °C at the same time, and the heating curves of the four materials were recorded. Then, when the temperature of all the test tubes was raised to 55 °C, the test tubes were removed simultaneously and placed in a constant temperature incubator at 15 °C, and the cooling curves of the four materials were recorded.

From Figure 14a, it can be seen that, under the thermal disturbance of 55 °C, the cement mortar, LA−MA, LA−PA, and LA−SA took 113, 350, 483, and 500 s to rise from 15 to 55 °C, respectively. LA−MA, LA−PA, and LA−SA took about 3.10×, 4.27×, and 4.43× longer than cement mortar, respectively. Similarly, from Figure 14b, it can be obtained that the cement mortar, LA−MA, LA−PA, and LA−SA took 383, 1507, 1425, and 1432 s to drop from 55 to 15 °C, respectively. LA−MA, LA−PA, and LA−SA took about 3.94×, 3.72×, and 3.74× longer than cement mortar, respectively. Based on these data, we can conclude that the time spent by lauric acid-based binary eutectic PCMs is significantly longer than that of cement mortars for both the heating and the cooling processes. This means that lauric acid-based eutectic PCMs have a strong thermal insulation and heat preservation effects, and combining them with the building envelope will certainly enhance the heat storage

https://doi.org/10.1021/acsomega.2c01420
ACS Omega 2022, 7, 16097−16108

capacity of the building envelope, thus achieving energy saving in buildings.

3.8. Thermal Stability of LA-Based Binary Eutectic PCMs. Thermal stability is critical to the practical application of composite materials. The thermal stabilities of LA−MA, LA−PA, and LA−SA eutectic PCM are performed by using TG equipment under a nitrogen atmosphere. Figure 15 showed the TG and DTG curves of LA−MA, LA−PA, and LA−SA binary eutectic PCMs, and the mass loss of the samples at typical temperatures are listed in Table 3.

Table 3. Mass Loss Rates of Samples at Typical Temperatures

	temperature (°C)				
PCMs	100	150	200	250	300
LA−MA	0	0.718%	12.234%	85.588%	99.656%
LA−PA	0	0.754%	18.646%	97.016%	99.180%
LA−SA	0	0.922%	14.681%	86.156%	99.260%

As can be seen from Figure 15, LA−MA, LA−PA, and LA−SA binary eutectic PCMs are single-stage decompositions. According to Figure 15a, LA−MA shows a single-stage mass loss that started at 126.51 °C, the maximum speed was at 248.39 °C and finished at 258.13 °C, which represents the decomposition of LA−MA. Similarly, as can be seen from Figure 15b, LA−PA also shows a single-stage mass loss that started at 135.7 °C, the maximum speed was at 235.41 °C and terminated at 252.59 °C, representing the decomposition of LA−PA. Furthermore, as shown in Figure 15c, for LA−SA, when the temperature is 110.08 °C, it starts to decompose. When the temperature is 241.19 °C, the decomposition rate is the largest. When the temperature is 276.25 °C, the material is basically completely decomposed. The initial decomposition temperatures of the three eutectic mixtures are greater than 100 °C, which means that LA−MA, LA−PA, and LA−SA eutectic PCMs have good thermal stability and meet the requirements of building materials.

3.9. Reliability of LA-Based Binary Eutectic PCMs. The thermal reliability of material is essential to assessing the service life of the material, hence, the thermal reliability of LA-based binary eutectic PCMs was analyzed by the thermal cycle test. Figure 16 provides the DSC curves of LA−MA, LA−PA, and LA−SA eutectic PCMs at the 1st, 100th, 200th, 300th, and 500th cycles, respectively. Moreover, the corresponding phase transition temperature and latent heats are listed on Table 4.

As shown in Figure 16, the DSC curves of LA−MA, LA−PA, and LA−SA eutectic PCMs show slight changes in shape or magnitude, and there are no new endothermic and exothermic peaks. According to the data in Table 4, during 500 cycles, the maximum absolute deviations of the melting temperatures of LA−MA, LA−PA, and LA−SA are 0.54, 0.81, and 0.75 °C, and the corresponding relative deviations are 1.54%, 2.18%, and 1.91%, respectively. Furthermore, the maximum absolute deviations of the melting enthalpy are 8.82, 15.66, and 13.65 J·g^{-1}, and the corresponding relative deviations are 5.31%, 8.55%, and 7.20%, respectively. In the same way, the maximum absolute deviations of the freezing temperature of LA−MA, LA−PA, and LA−SA are 0.59, 0.47, and 0.31 °C, and the corresponding relative deviations are 1.84%, 1.5%, and 0.96%, respectively. Meanwhile, the maximum absolute deviations of the freezing enthalpy are 9.41, 10.89, and 15.94 J·g^{-1}, and the corresponding relative deviations are 5.94%, 6.53%, and 9.05%, respectively. The relative deviation of the phase change temperature of all binary PCMs is less than 3%, and its enthalpy is less than 10%. These changes in melting temperature and enthalpy are most likely due to the presence of impurities.[16,33,34] There are two possible mechanisms of action of impurities: one is the physical interaction of impurities with lauric acid-based eutectic PCM, and these interactions cause irregular changes of temperature and enthalpy. The other one is that impurities affect the DSC measurement results.[35] We also note that the solidification

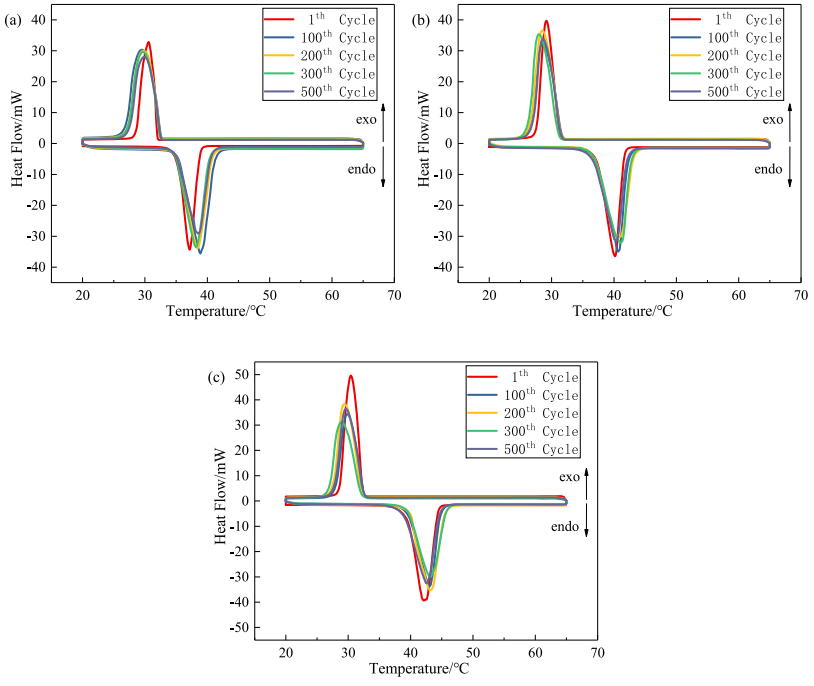

Figure 16. DSC curves of (a) LA−MA, (b) LA−PA, and (c) LA−SA eutectic PCMs during 1, 100, 200, 300, and 500 cycles tests.

https://doi.org/10.1021/acsomega.2c01420
ACS Omega 2022, 7, 16097−16108

Table 4. Thermal Properties of LA−MA, LA−PA, and LA−SA Eutectic PCMs During 1, 100, 200, 300, and 500 Cycles Tests[a]

		No. of cycling tests						
eutectic PCMs		1	100	200	300	500	maximum absolute deviation	maximum relative deviation
LA−MA	T_m (°C)	35.10	35.03	34.86	34.56	34.66	0.54	1.54%
	ΔH_m (J·g^{-1})	166.18	159.28	160.23	158.79	157.36	8.82	5.31%
	T_f (°C)	32.15	32.74	32.66	32.57	32.68	0.59	1.84%
	ΔH_f (J·g^{-1})	158.43	151.47	149.02	152.10	151.29	9.41	5.94%
LA−PA	T_m (°C)	37.15	36.48	36.55	36.65	36.34	0.81	2.18%
	ΔH_m (J·g^{-1})	183.07	168.25	177.48	174.30	167.41	15.66	8.55%
	T_f (°C)	31.34	31.81	31.69	31.29	31.69	0.47	1.50%
	ΔH_f (J·g^{-1})	166.81	155.92	162.16	158.10	157.29	10.89	6.53%
LA−SA	T_m (°C)	39.29	39.18	39.51	39.24	38.54	0.75	1.91%
	ΔH_m (J·g^{-1})	189.50	176.81	183.85	177.82	175.85	13.65	7.20%
	T_f (°C)	32.44	32.75	32.42	32.25	32.68	0.31	0.96%
	ΔH_f (J·g^{-1})	176.15	160.21	165.55	161.37	163.05	15.94	9.05%

[a] T_m is the melting temperature ; ΔH_m is the melting enthalpy; T_f is the freezing temperature; ΔH_f is the freezing enthalpy.

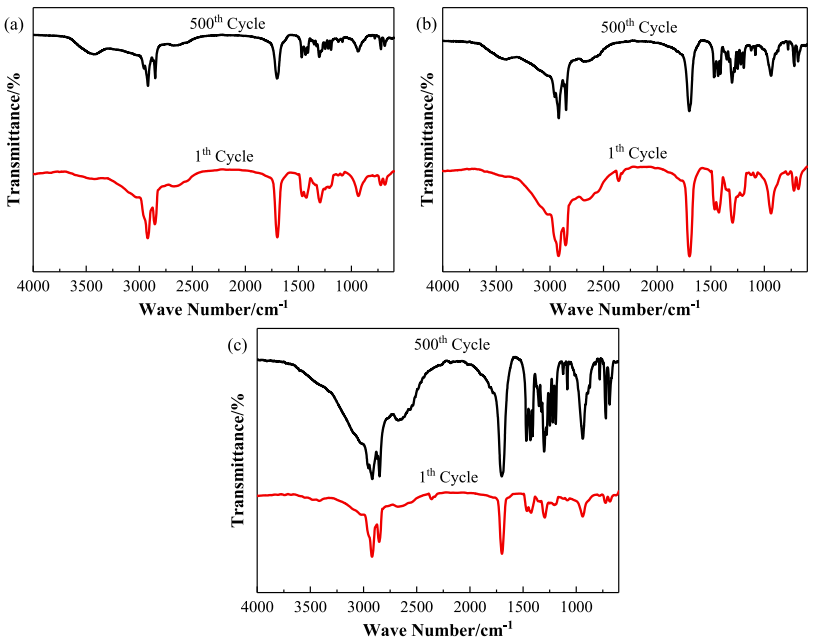

Figure 17. FT-IR spectra of the 1st and 500th cycles: (a) LA−MA, (b) LA−PA, and (c) LA−SA eutectic PCMs.

enthalpy of LA−SA varies more than that of LA−MA and LA−PA, which is due to the fact that SA has more impurities than PA and MA. However, the slight changes in phase change temperature and enthalpy are acceptable in building energy conservation. The results demonstrate that these LA-based binary eutectic PCMs have good thermal reliability during a long-time application as a PCM.

FT-IR was utilized to evaluate the chemical reliability of LA-based eutectic PCMs. The FT-IR spectra of the 1st and 500th cycles of LA−MA, LA−PA, and LA−SA eutectic PCMs are presented in Figure 17. As shown in Figure 17, for these binary eutectic PCMs, it can be found that the peak shape and absorption band of functional groups are the same as before the cycle. This phenomenon shows that LA−MA, LA−PA, and LA−SA have good chemical reliability in practical applications.

4. CONCLUSIONS

Thermal properties, stabilities, and reliabilities of lauric acid-based binary eutectic mixtures for building energy efficiency were studied. The step cooling curve experiment confirmed the eutectic points of the lauric acid-based binary eutectic mixtures. The eutectic compositions are $\mathcal{M}_{LA}$ = 70%, $\mathcal{M}_{LA}$ = 79%, and $\mathcal{M}_{LA}$ = 82% with melting temperatures of 35.10, 37.15, and 39.29 °C, and latent heats of melting are found to be ΔH_m = 166.18, 183.07, and 189.50 J·g^{-1} for the LA−MA, LA−PA, and LA−SA binary eutectic PCMs, respectively. The melting temperature, eutectic point, and melting enthalpy of LA−MA, LA−PA, and LA−SA binary PCMs were calculated according to Schroder's formula. The results indicated that the theoretical calculation value and the experimental value are in good agreement. Furthermore, the FT-IR and XRD analyses indicated that there was no chemical reaction in the preparation of the LA−MA eutectic PCMs, LA−PA eutectic PCMs, and LA−SA eutectic PCM eutectic mixtures, respectively, and the componentshave good compatibility. Besides, the TG and cycle test illustrate that the LA−MA eutectic PCMs, LA−PA eutectic PCMs, and LA−SA eutectic PCMs exhibit excellent thermal stability and reliability below 126.51, 135.7, and 110.08 °C, respectively. In conclusion, the LA-based binary eutectic PCMs are competitive insulation materials for building energy conservation.

https://doi.org/10.1021/acsomega.2c01420
ACS Omega 2022, 7, 16097−16108

AUTHOR INFORMATION

Corresponding Author

Yunchao Zhao − *Jiangxi Province Key Laboratory of Environmental Geotechnical Engineering and Hazards Control, Jiangxi University of Science and Technology, Ganzhou 341000 Jiangxi Province, China;* orcid.org/0000-0001-9088-4601; Email: 465654315@qq.com

Authors

Zhixuan Fan − *Jiangxi Province Key Laboratory of Environmental Geotechnical Engineering and Hazards Control, Jiangxi University of Science and Technology, Ganzhou 341000 Jiangxi Province, China;* orcid.org/0000-0003-2737-7820

Xuying Liu − *Jiangxi Province Key Laboratory of Environmental Geotechnical Engineering and Hazards Control, Jiangxi University of Science and Technology, Ganzhou 341000 Jiangxi Province, China*

Yu Shi − *Jiangxi Province Key Laboratory of Environmental Geotechnical Engineering and Hazards Control, Jiangxi University of Science and Technology, Ganzhou 341000 Jiangxi Province, China*

Dahua Jiang − *Jiangxi Province Key Laboratory of Environmental Geotechnical Engineering and Hazards Control, Jiangxi University of Science and Technology, Ganzhou 341000 Jiangxi Province, China;* orcid.org/0000-0002-4677-6985

Complete contact information is available at: https://pubs.acs.org/10.1021/acsomega.2c01420

Notes

The authors declare no competing financial interest.

ACKNOWLEDGMENTS

The authors would like to thank the Science and Technology Research Project of Jiangxi Provincial Department of China (No. GJJ200830) and Jiangxi University of Science and Technology High-Level Talents Research Start-up Project (2021205200100553).

REFERENCES

(1) Cantore, N.; Schlor, H.; Voegele, S.; Kuckshinrichs, W.; Haraguchi, N.; Nussbaumer, P.; Yan, J. Inclusive and sustainable industrial development: Measurement approaches for energy transformation. *Appl. Energy* **2021**, *299*, 117277.

(2) Guo, H. D.; Zhang, Y. X.; Zhao, Q. Q.; REN, S. M. International government regulatory experience of building energy-saving: A survey. *Ecological Economy* **2017**, *3*, 291−300.

(3) He, Y.; Zhang, X.; Zhang, Y. Preparation technology of phase change perlite and performance research of phase change and temperature control mortar. *Energy Buildings* **2014**, *85*, 506−514.

(4) Castell, A.; Martorell, I.; Medrano, M.; Pérez, G.; Cabeza, L. F. Experimental study of using PCM in brick constructive solutions for passive cooling. *Energy Buildings* **2010**, *42* (4), 534−540.

(5) Zhang, Y.; Deng, M. Taguchi optimization and a fast evaluation method on the transient thermal performance of phase change material outfitted walls. *J. Energy Storage* **2021**, *43*, 103120.

(6) Qiao, X.; Kong, X.; Li, H.; Wang, L.; Long, H. Performance and optimization of a novel active solar heating wall coupled with phase change material. *J. Cleaner Prod.* **2020**, *250*, 119470.

(7) Jin, X.; Zhang, X. Thermal analysis of a double layer phase change material floor. *Appl. Therm. Eng.* **2011**, *31* (10), 1576−1581.

(8) Alim, M. A.; Tao, Z.; Abden, M. J.; Rahman, A.; Samali, B. Improving performance of solar roof tiles by incorporating phase change material. *Sol. Energy* **2020**, *207*, 1308−1320.

(9) Schaink, H. M.; Van Malssen, K. F.; Morgado-Alves, S.; Kalnin, D.; Van der Linden, E. Crystal network for edible oil organogels: possibilities and limitations of the fatty acid and fatty alcohol systems. *Food Res. Int.* **2007**, *40* (9), 1185−1193.

(10) Daniel, J.; Rajasekharan, R. Organogelation of plant oils and hydrocarbons by long-chain saturated FA, fatty alcohols, wax esters, and dicarboxylic acids. *J. Am. Oil Chem. Soc.* **2003**, *80* (5), 417−421.

(11) Feldman, D.; Shapiro, M. M.; Banu, D.; Fuks, C. J. Fatty acids and their mixtures as phase-change materials for thermal energy storage. *Sol. Energy Mater.* **1989**, *18* (3−4), 201−216.

(12) Rozanna, D.; Chuah, T. G.; Salmiah, A.; Choong, T. S.; Sa'Ari, M. Fatty acids as phase change materials (PCMs) for thermal energy storage: a review. *Int. J. Green Energy* **2005**, *1*, 495−513.

(13) Cedeño, F. O.; Prieto, M. M.; Espina, A.; Garcıa, J. R. Measurements of temperature and melting heat of some pure fatty acids and their binary and ternary mixtures by differential scanning calorimetry. *Thermochim. Acta* **2001**, *369*, 39−50.

(14) Inoue, T.; Hisatsugu, Y.; Ishikawa, R.; Suzuki, M. Solid-liquid phase behavior of binary fatty acid mixtures: 2. Mixtures of oleic acid with lauric acid, myristic acid, and palmitic acid. *Chem. Phys. Lipids* **2004**, *127*, 161−173.

(15) Principi, P.; Fioretti, R. Thermal analysis of the application of PCM and low emissivity coating in hollow bricks. *Energy Buildings* **2012**, *51*, 131−142.

(16) Yang, L.; Cao, X.; Zhang, N.; Xiang, B.; Zhang, Z.; Qian, B. Thermal reliability of typical fatty acids as phase change materials based on 10,000 accelerated thermal cycles. *Sustain. Cities. Soc.* **2019**, *46*, 101380.

(17) Yuan, Y.; Zhang, N.; Tao, W.; Cao, X.; He, Y. Fatty acids as phase change materials: a review. *Renewable Sustainable Energy Rev.* **2014**, *29*, 482−498.

(18) Saeed, R. M.; Schlegel, J. P.; Castano, C.; Sawafta, R.; Kuturu, V. Preparation and thermal performance of methyl palmitate and lauric acid eutectic mixture as phase change material (PCM). *J. Energy Storage* **2017**, *13*, 418−424.

(19) Wen, R.; Zhang, X.; Huang, Y.; Yin, Z.; Huang, Z.; Fang, M.; Liu, Y.; Wu, X. Preparation and properties of fatty acid eutectics/expanded perlite and expanded vermiculite shape-stabilized materials for thermal energy storage in buildings. *Energy Buildings* **2017**, *139*, 197−204.

(20) Kahwaji, S.; Johnson, M. B.; Kheirabadi, A. C.; Groulx, D.; White, M. A. Stable, low-cost phase change material for building applications: the eutectic mixture of decanoic acid and tetradecanoic acid. *Appl. Energy* **2016**, *168*, 457−464.

(21) Han, L.; Ma, G.; Xie, S.; Sun, J.; Jia, Y.; Jing, Y. Thermal properties and stabilities of the eutectic mixture: 1, 6-hexanediol/lauric acid as a phase change material for thermal energy storage. *Appl. Therm. Eng.* **2017**, *116*, 153−159.

(22) Zhou, D.; Zhao, C. Y.; Tian, Y. Review on thermal energy storage with phase change materials (PCMs) in building applications. *Appl. Energy* **2012**, *92*, 593−605.

(23) Yu, J.; Yang, Q.; Ye, H.; Huang, J.; Liu, Y.; Tao, J. The optimum phase transition temperature for building roof with outer layer PCM in different climate regions of China. *Energy Procedia* **2019**, *158*, 3045−3051.

(24) Ye, R.; Huang, R.; Fang, X.; Zhang, Z. Simulative optimization on energy saving performance of phase change panels with different phase transition temperatures. *Sustain. Cities. Soc.* **2020**, *52*, 101833.

(25) He, Y.; Zhang, X.; Zhang, Y. Preparation technology of phase change perlite and performance research of phase change and temperature control mortar. *Energy Buildings* **2014**, *85*, 506−514.

(26) Hekimoğlu, G.; Nas, M.; Ouikhalfan, M.; Sarı, A.; Kurbetci, Ş.; Tyagi, V. V.; Sharma, R. K.; Saleh, T. A. Thermal management performance and mechanical properties of a novel cementitious composite containing fly ash/lauric acid-myristic acid as form-stable phase change material. *Constr. Build. Mater.* **2021**, *274*, 122105.

https://doi.org/10.1021/acsomega.2c01420
ACS Omega 2022, 7, 16097−16108

(27) Sarı, A. Eutectic mixtures of some fatty acids for low temperature solar heating applications: Thermal properties and thermal reliability. *Appl. Therm. Eng.* **2005**, *25*, 2100−2107.
(28) Ke, H. Phase diagrams, eutectic mass ratios and thermal energy storage properties of multiple fatty acid eutectics as novel solid-liquid phase change materials for storage and retrieval of thermal energy. *Appl. Therm. Eng.* **2017**, *113*, 1319−1331.
(29) Ke, H.; Pang, Z.; Peng, B.; Wang, J.; Cai, Y.; Huang, F.; Wei, Q. Thermal energy storage and retrieval properties of form-stable phase change nanofibrous mats based on ternary fatty acid eutectics/polyacrylonitrile composite by magnetron sputtering of silver. *J. Therm. Anal. Calorim.* **2016**, *123*, 1293−1307.
(30) Liu, C.; Yuan, Y. P.; Zhang, N.; Cao, X. L.; Yang, X. J. Theoretic prediction of phase change temperature and latent heat of fatty acids ternary eutectic mixture. *Materials Review* **2014**, *28*, 165−168.
(31) Sarier, N.; Onder, E. Organic phase change materials and their textile applications: an overview. *Thermochim. Acta* **2012**, *540*, 7−60.
(32) Cárdenas-Ramírez, C.; Gómez, M. A.; Jaramillo, F. Comprehensive analysis of the thermal properties of capric-myristic, lauric-myristic and palmitic-stearic acids and their shape-stabilization in an inorganic support. *J. Energy Storage* **2021**, *34*, 102015.
(33) Sharma, A.; Sharma, S. D.; Buddhi, D. Accelerated thermal cycle test of acetamide, stearic acid and paraffin wax for solar thermal latent heat storage applications. *Energy Convers. Manage.* **2002**, *43*, 1923−1930.
(34) San, A. Thermal reliability test of some fatty acids as pcms used for solar thermal latent heat storage applications. *Energy Convers. Manage.* **2003**, *44*, 2277−2287.
(35) Zhang, L.; Dong, J. Experimental study on the thermal stability of a paraffin mixture with up to 10,000 thermal cycles. *Therm. Sci. Eng. Prog.* **2017**, *1*, 78−87.

https://doi.org/10.1021/acsomega.2c01420
ACS Omega 2022, 7, 16097−16108